Chapter 2

Methodology

Be more dedicated to making solid achievements than in running after swift but synthetic happiness.

- Dr. A.P.J. Abdul Kalam

CHAPTER 2 METHODOLOGY

2.1 Field Investigations

Landscape is a net result of competition that takes place between the climate driven surface processes and tectonics that is linked to earth's interior as well as what's happening in the hinterland and in the sink area. These forces leave their signatures in the geomorphic and depositional architecture of a landscape in a very subtle way. Therefore, in order to understand the genesis of any landscape, the knowledge of the geology, geomorphology and careful field observations are very important. The geological field work in Ladakh Himalaya, an environmentally stressed terrain, was carried out to understand late Quaternary landscape evolution and its relationship with climate/tectonics. The sedimentological, geomorphological and geochronological studies on fluvial landforms of the Indus River from Nyoma to Dah – Hanu and sand ramps in Leh valley was done during two field seasons of total 63 days.

2.2 Geomorphic studies

Prior to the field work, a geomorphic overview of the Ladakh Himalaya was investigated using Google Earth, Advance Spaceborne Thermal Emission and Reflection Radiometer (ASTER), and Survey of India (SOI) maps. In the field, the fill terraces were measured with a tape and detailed lithologs were prepared. The height of strath terraces with respect to the riverbed was determined by using Total

Station (South NTS 352, resolution: 3"). The reference height for total station survey was taken from hand GPS (Global Positioning System) having accuracy of ± 3 m)

The Digital Elevation Model (DEM) of Shuttle Radar Topographic Mission (SRTM) of 3 arc second resolution, ASTER, resolution 1 arc second, and SOI topographic sheets (1:50000) were used to study river pattern changes, valley cross-sections and longitudinal river profile. To prepare longitudinal river profile, the projection of SRTM DEM was changed from 'WGS 84' to 'Lambert Conformal Conic' to transform the units from degree to meter. The Environmental System Research Institute's (ESRI) ArcGIS 9.3 software was used for all corrections and data processing. A hydrological tools of ArcGIS and standard protocols were adopted to generate the stream from DEM. The small channels which have pixel values less than the trunk channel were deleted and all fragments were merged to form one line feature (stream). The whole length of the trunk channel was segmented and separated by a pixel size of SRTM DEM (90 m). These line features then converted into points and added with field x, y (lat., long.). The z values (Raster values) were extracted from the DEM in the attribute table using 'extract values to the points' tool. Further, the attribute table was exported in text format and used to compute the longitudinal river profile and Stream length (SL) gradient index of the Indus River.

There are many morphometric indices, to understand the geomorphological fingerprints and landform evolution along a stream. In spite of that, the longitudinal river profile and associated indices are widely used to understand the tectonic

activity. Stream length (SL) gradient index and concavity index (K_{sn}) are popularly used to delineate the zones of tectonic perturbations. K_{sn} index has a power relationship with channel gradient and drainage basin area, and it can be used to quantify the knickpoints and possible causes behind the formation in any landscape. However, in K_{sn} studies the basic assumption is uniform spatial uplift rate, which is often questioned (Whipple and Tucker, 1999). This method, thus, do not incorporate nonlinearities in tectonic driven incision processes (Whipple et al., 2000) and channel morphology (Lavé and Avouac, 2000, 2001), riverbed state (Hancock and Anderson, 2002; Whipple and Tucker, 2002) etc. The SL index on the other hand, is associated with the total stream power, its flow resistance and erodibility contrast at a particular reach, which further can be correlated with lithological changes and tectonic activities. Therefore, the SL index can be used as a practical tool and important parameter for this study.

Stream length (SL) gradient index was calculated for complete course of the river i.e. Nyoma to Dah Hanu (~ 350 km) using the following mathematical expression given by Hack (1973),

$$SL = \frac{H1 - H2}{\ln L2 - \ln L1}$$

The H_1, H_2 are the elevation (m) from mean sea level for the points situated at distance L_1 and L_2 from the source.

For sand ramp mapping, the ASTER DEM and the google earth images were used. Twenty one sand ramps were mapped on google earth using polygon tool. The *.kml*

files of mapped polygons then converted into *.shape* files and stapled on ASTER DEM. Before affixing, the projection of DEM converted from 'WGS84' to 'Lambert conformal conic' by following the steps explained above. The Area, slope and aspect of an individual sand ramp was estimated by applying 'Topographic analysis tool' in ERDAS IMAGINE 11 by defining equal projection on all sand ramps *.shape* files and DEM.

2.3 Lithofacies analysis of terrace sequences

In the field, sedimentary archives of fill terraces, fans and sand ramps were investigated using widely used sedimentary techniques. The valley fills were studied using vertical and lateral lithologs. The exposed sections were taken into account for lithofacies classification, clast counting and terrace mapping. Identification of lithofacies is done by observing physical structures, clast size, roundness, sorting, imbrication, clast lithology, matrix percentage and its grain size, lateral geometry of the unit and biogenic activities such as bioturbation etc. The clast composition and textural data was determined by superimposing the 1×1 m grid on exposed sections.

2.4 Chronology

A number of dating techniques which can provide the time span of deposition and demarcate the incision events of rivers exist. Techniques using Accelerator Mass Spectrometer (AMS) on ^{14}C of organic material, often used in the Quaternary studies, suffers from a range of problems *viz.* (i) contamination from older or

younger carbon, (ii) upper datable limit being not more than 50 ka, and (iii) poor occurrence of organic matter in arid zones. In the present study we have used luminescence dating technique that is globally used to date range of material in Quaternary geology. This technique is used to date depositional events using quartz and feldspar that are communing occurring minerals in the sediments. The Luminescence dating technique can provide chronology to the depositional event has a dating limit from few tens of years to few hundreds of years. This technique has vast application in (i) fluvial, alluvial, aeolian, glacio – fluvial sediments, (ii) archaeology, and (iii) determining the activity of fault during the late Quaternary etc. Our study is oriented in and around the fluvial, alluvial, aeolian and glaciogenic landforms, therefore the optical dating suited most to setup the chronology of landforms.

2.4.1 Introduction to Luminescence Dating and Principle

The luminescence is an emission of light from any substance when stimulated by an external source of energy such as light or heat. The luminescence dating is based on the concept that natural minerals can absorb and store energy (any form of energy; Lian, 2007). The exposure to light or heat can bleach completely or reduce the energy stored in natural minerals. The common minerals associated with luminescence dating are quartz and feldspar. The reason being; (1) these minerals are abundant in any type of sediment, and (2) the physical and optical properties of these minerals are well understood.

The principle of luminescence dating can further be understood by the band theory for the solids i.e. electrons stored in the lower energy level (valence band) jump to the higher energy level (conduction band) after getting flux of radiation energy. These radiation fluxes can be provided by the radioactive decay of U, Th and K which are present in the sediments. The cosmic radiations also adds to this flux in the form of Gamma. In the higher energy level the electrons are unstable and these, thus, get diffused to lower levels and stabilize by releasing some energy in the form of photons and subsequently get trapped below the conduction band. The lattice defects present in any crystal can act as trap centers. The usefulness of any trap depends upon its depth, in terms of energy below the conduction band. Higher the depth, higher will be the stability. These two steps are termed as irradiation and storage (Fig 2.1). Therefore any trapped electron will have a threshold energy € that will be required to evacuate that electron from a particular trap. The ejected electron can get attracted by recombination center, called as luminescence centers, instantaneously. The processes of diffusion and recombination of electrons into luminescence center emits light. This can be assisted by thermal or optical stimulation and depending upon this, the emitting light can be termed as thermoluminescence (TL) or optically stimulated luminescence (OSL) respectively (Aitken, 1998).

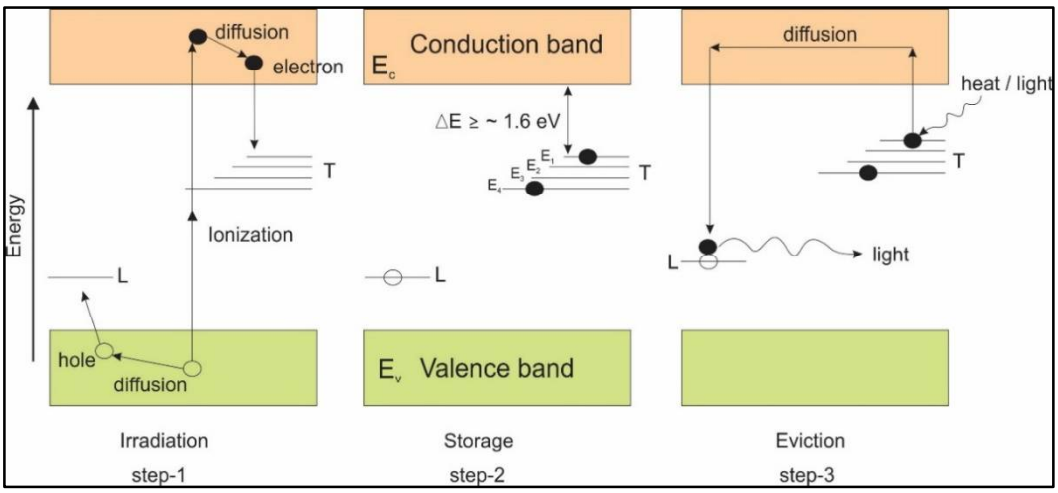

Figure 2.1 The energy level diagram explaining the TL/OSL working mechanism. In step-1, the ionization of the electrons occurred due to exposure of nuclear radiations. The formation of traps (T) and luminescence center (L) is due to movement of electrons and hole in the lattice of mineral, respectively. Step-2, represents the storage of electrons in the trap by continuous ionization. For dating, the life of trap should be more than the life of accumulation of electrons, therefore, the trap should not leak and hence the depth of trap should be equal to more than 1.6 eV. Step- 3, represents the eviction of electrons from the traps after get stimulated by suitable wavelength of light so that the electron get diffused into the conduction band and get attracted by the recombination center (luminescence center) to generate luminescence (Aitken, 1998).

In TL, the minerals are heated to a threshold temperature to evict the trapped electrons. In OSL, the eviction of electrons from the traps, depends upon the rate of arrival of photons and the emission counts. The eviction process depend on both,

the characteristics of trap as well as on the stimulating wavelength, shorter the wavelength more will be the eviction. The absorption of photon is inversely proportion to the stimulating wavelength.

$$Energy\ (eV) = \frac{1240}{wavelength\ (nm)}$$

Further, depending upon wavelength opted for stimulation, the OSL can be divided into Blue – Green stimulated luminescence (BGSL), 486 – 517 nm and Infrared stimulated luminescence (IRSL), 700 – 1400 nm. The basic stimulation light source used in luminescence dating system is blue and infrared LEDs having wavelength of 470±30 nm and 870±70 nm. For quartz, the trap depth with more than 1.7 eV has thermal stability (Wintle, 1997) that has enough binding energy to store the trapped electron as explained in figure 2.1, and maximum wavelength to which the eviction can occur is ~ 400 nm. It is presumed that the traps for the quartz having depth ~ 2.7 eV (~ 470 nm) are stable as far as OSL dating is concerned (Wintle, 1997). The optical dating of feldspars, which have variety of minerals, are being done using infrared (IR) stimulation. The feldspars having low thermal stability (1.45 eV) and have tendency of leaking trapped electron at room temperature via tunneling effect, this phenomenon is known as **anomalous fading.** Therefore, in case of feldspars fading corrections are needed to estimate the ages.

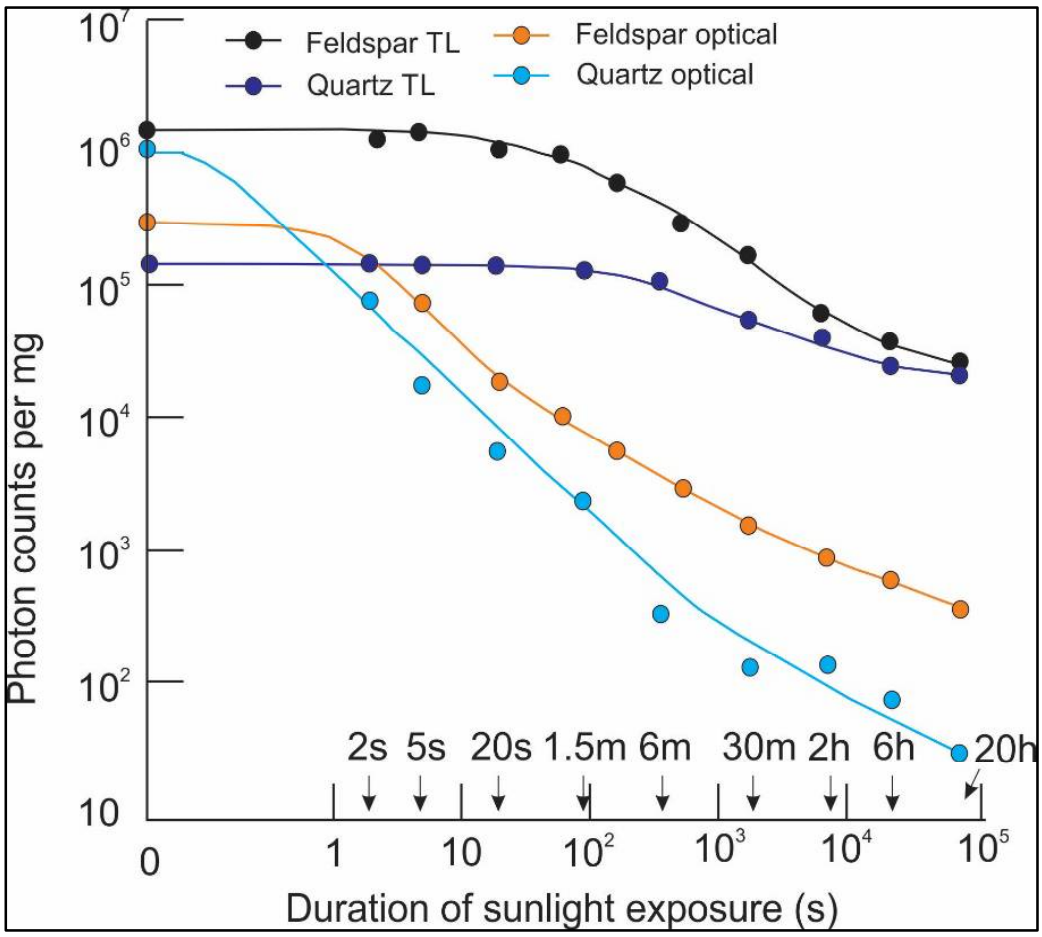

Figure. 2.2 Natural OSL and TL signals reduced in quartz and feldspar after exposure to sunlight. OSL has faster reduction than the TL in both quartz and feldspar (from Godfrey-Smith et al., 1988).

2.4.2 Optical bleaching and its relation with geological processes

The bleaching of signal is, when sediment is exposed to sunlight or any light, reduction in both TL and OSL signals. The spectra of sunlight which extends from ultraviolet to infrared, and covers the most wavelengths, is relevant to the bleaching. When the sediment is exposed to sunlight, all the trapped electrons are

evacuated and luminescence clock resets to zero. It is experimentally observed by Godfrey-Smith et al., (1988) that the OSL signals reduced much faster than the TL signals in quartz as well as in feldspar. Therefore, quartz bleaches more rapidly than feldspar.

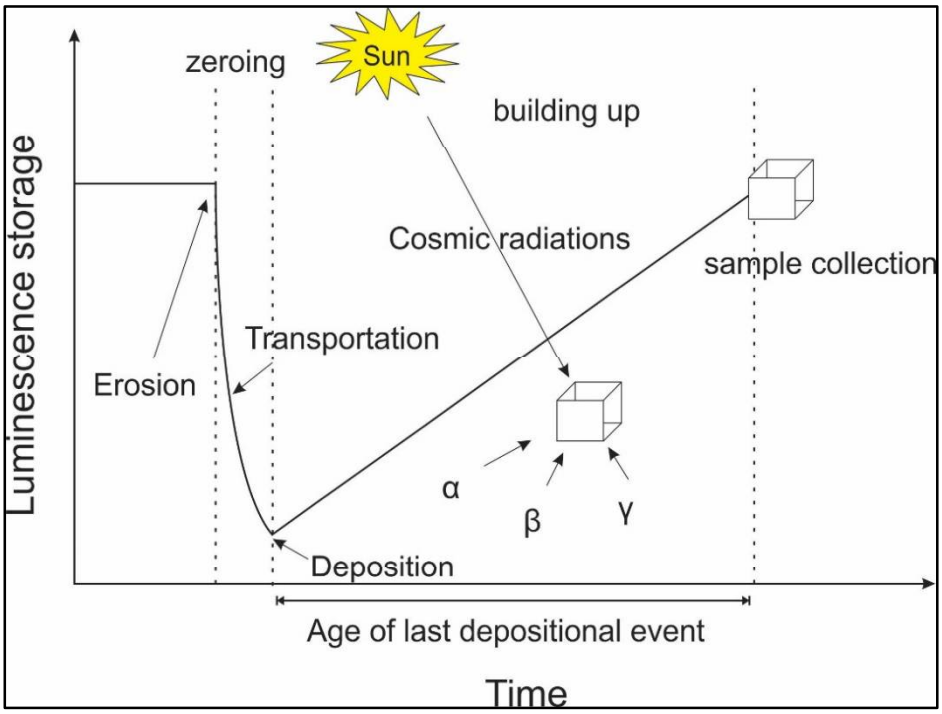

Figure 2.3 Schematic representation of the building up and zeroing of the luminescence signals in a sediment sample. The erosional and transportation processes reduces the luminescence through direct exposure to sunlight or daylight. The build-up of luminescence is through accumulation of electrons in traps by getting flux of radiations due to continuous decay of U, Th and K and supply α, β and γ radiations. The cosmic radiations helps in building-up the luminescence signals in the sample (modified after Wintle and Huntley, 1982; Lepper et al., 2001).

It is assumed, in the OSL dating that prior to burial, the geological luminescence is reduced to near zero. After deposition, in the presence of natural radioactivity and cosmic radiation the chronometers such as quartz and feldspars buildup the luminescence in their lattice (Fig 2.3). Subsequent to sampling and laboratory procedures, the estimated palaeodose equals to this built up luminescence. Hence the OSL actually dates the last burial event.

In the present study samples were collected in order to constrain the start and termination of valley filling process and the formation of terraces. The alluvial covers of the strath terraces were sampled to understand the uplift rates and bedrock incision rates.

2.4.3 Optically Stimulated Luminescence and age evaluation

The light emitted due to optical stimulation is known as optically stimulated luminescence (OSL). The OSL ages therefore are based on estimation of two parameters; (i) the total accumulated dose whose laboratory equivalent is called as palaeodose or Equivalent dose or ED, and (ii) the rate at which this dose accumulated in the chronometer i.e. dose rate. Therefore the equation for age evaluation is

$$Age = \frac{Palaeodose}{Dose\ rate}$$

The palaeodose is measured in Gray (Gy) = 1 J kg^{-1} and dose rate are in Grays per thousand years (Gy ka^{-1}). The radiation that impart palaeodose are α, β and γ that can penetrate in the range of 10-30 μm, 3 mm and 0.3 – 0.8 m, respectively, therefore, the γ radiations pass through the sedimentary grains without exciting the

electrons present in the valance band. In fine sand (150 μm), only α and β contribute, whereas γ is least ionizing and α ionizes the thin skin heavily. Therefore, α effected skin (10-20 μm) is removed and thus the grains are subjected to etch with Hydro fluoric (HF) acid. The fourth radiations, cosmic radiations, also contributes to some extent and therefore the age equation can be written more precisely as:

$$Age = \frac{Palaeodose}{0.90D_{\beta} + D_{\gamma} + D_{c}}$$

D_{β}, D_{γ} and D_c are the dose rate due to β, γ and cosmic radiations. The 0.90 factor arises due to attenuation in β.

2.4.3.1 Environmental dose rate determination

U, Th and K contents in the bulk sediment samples were measured using X-ray Fluorescence (XRF) or Inductively Coupled Plasma Mass Spectroscopy (ICP-MS) methods and the dose contribution was estimated using Table 2.1 that is in built, in age calculation software of Grün. The presence of moisture also affect the dose rate. A thin film of moisture present in the pores of sediment can attenuate the radiation coming from U, Th and K and as a result reduce the effective dose rate. As Ladakh Himalaya (study area) is a cold and semi- arid zone with annual precipitation ~100 mm/a, the moisture content taken into account in these samples were 5±3 % by weight. At altitude of ≥3000 m msl, the cosmic dose is also significant and was estimated as per Prescott and Stephan (1982).

Table 2.1 The doserate contribution by different radioactive element in Gy ka^{-1} (Aitken, 1998)

S No.	Element	Concentration	Effective Dose rates (Gy ka^{-1})		
			α	β	γ
1	Uranium (U)	1 ppm	0.231	0.145	0.113
2	Thorium (Th)	3 ppm	0.193	0.082	0.143
3	Potassium (K)	1 %	--	0.782	0.243
4	Rubidium (Rb)	50 ppm	--	0.019	--
5	Cosmic	--	--	--	0.18
6	Due to the presence of 10 % moisture the Attenuation factor is		1.15	1.125	1.114

2.4.3.2 Palaeodose estimation

The palaeodose estimation, requires the comparison of laboratory dose to that acquired naturally. In this study the most widely used protocol, Single Aliquot Regeneration (SAR), is applied. To estimate palaeodose using SAR protocol, a mono layer of quartz (75- 125 μm) was mounted on stainless steel disc having diameter of 9.6 mm. Each aliquot is then preheated at 200 °C to 260 °C, before

measuring the response of natural and regenerative doses. The sensitivity is checked at every step of natural and regenerative dose by giving a small fixed dose (known as test dose) and subsequent cut heat. The preheat temperature was selected by testing a number of samples using Preheat Plateau Test and Dose Recovery Test (Fig 2.6). 220 ºC preheat temperature for 10s and 160 ºC cut heat was found most suitable for Ladakh samples (Murray and Wintle, 2000).

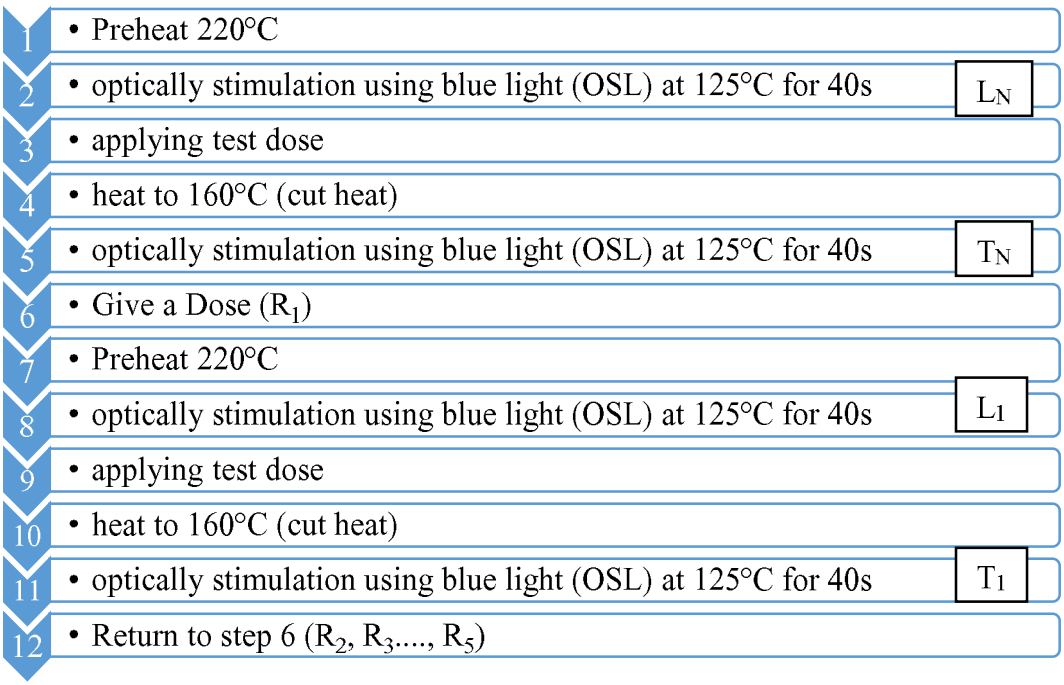

Figure 2.4 The schematic algorithm for SAR protocol. L_N and T_N are natural and test dose luminescence, L_1 and T_1 are luminescence measured after first incremental dose followed by test dose. This protocol is also known as five points SAR protocol because it has three incremental dose followed by one zero dose and one repetition of any incremental dose.

A schematic algorithm used to evaluate palaeodose from SAR protocol (Murray and Wintle, 2000) is given in figure 2.4. The sediments from the Himalaya often have a problem of feldspar contamination which is checked by performing feldspar test using IRSL. The sample contaminated with the feldspar usually yields high IRSL counts otherwise the counts remain < 150. In case of contamination an additional step of 10 min etching and/or optically stimulation using infrared (IRSL) at 60 °C for 100s is introduced before OSL readout and the method is known as double SAR protocol (Jain and Singhvi, 2001).

The OSL is measured at 125 °C for 40s. L_N, T_N are the natural and test dose luminescence, whereas L_N/T_N gives the sensitively corrected luminescence. In figure 2.4, the step 6 and 11, representing the luminescence of first regenerative dose (L_1) and test dose (T_1), respectively. The successive increment doses and measurement were done from steps from 6 to 11 (R_2, R_3, R_4 and R_5). R_4 is the regeneration at zero dose to check the recuperation. R_5 measured by repeating the first incremental dose to check the reproducibility and is estimated in terms of recycling ratio. The L_1/ T_1, L_2/ T_2…, L_5/ T_5 represent the sensitivity corrected luminescence of respective R_1, R_2…, and R_5 and plotted to generate growth curve to evaluate palaeodose of respective sample.

2.4.4 Laboratory procedures

In the field, the sediment was sampled in a ~ 9" long and ~ 3" diameter opaque stainless steel tubes. During sampling, tubes were inserted horizontally by hammering in sand units. In laboratory, the samples were opened in subdued red

light. A few centimeter sediment at both ends of the pipe, had potentially exposed to sunlight during sampling, were removed and utilized for U, Th and K estimation.

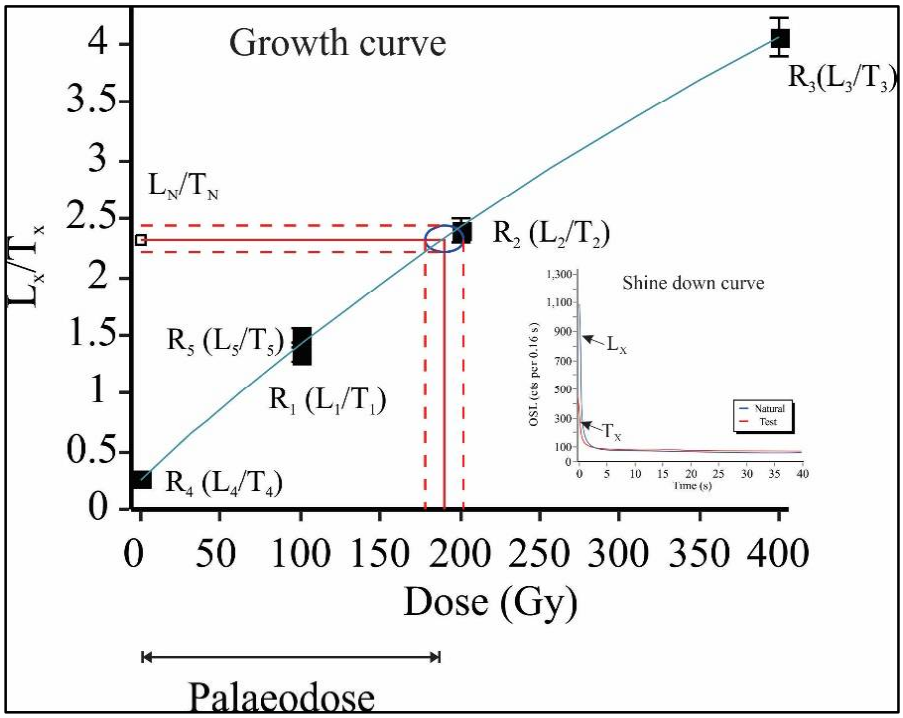

Figure 2.5 The sensitivity corrected luminescence are plotted against the given incremental doses to generate growth curve. A straight line which cuts the growth curve from natural dose, when extended perpendicularly to dose axis, gives palaeodose. The inset shows the shine down curve for natural and test doses.

The middle unexposed portion of the sample was dried and sieved. After this, 90 to 125 µm fraction were treated with 1 N HCl to digest carbonate and 30% H_2O_2 to remove organic matter (Aitken, 1998; Srivastava et al., 2006, 2008). Following this, the sample was washed with distilled water to remove all acid. After

drying the sample in an oven (<60° C), it was subjected to heavy liquid density separation to separate quartz (solution of Sodium poly tungstate). Since quartz has density of 2.65 g/cm^3, the density of the liquid (solution of Sodium poly tungstate) 2.67 g/cm^3 and 2.62 g/cm^3 density were used to separate quartz from heavy minerals and feldspars. The separated quartz was subjected to etching with 40% HF for 80 min followed by 20 min treatment with 12 N HCl to remove 10 – 15 μm α – affected skin.

The IRSL measurement was carried for every sample to check the feldspar content, if the IRSL counts were more than 150 counts, then the samples were additionally etched for 10 min using 40 % HF and 10 min treatment with 12 N HCl. The clean quartz grains were stacked on steel discs using SLIKOSPRAY silicon oil and run to evaluate palaeodose.

2.4.5 Instrumentation and OSL measurement

The luminescence of quartz and feldspar grains was measured on Riso TL/ OSL-20 system with arrays of blue (470±30 nm) and infrared LEDs (870±70 nm), respectively. The total power supplied by the blue and infrared LEDs were 45 mW/cm^2 and 145 mW/cm^2 to the sample position. The quartz grain was stimulated at 125 °C elevated temperature for 40 s. The feldspar grains were stimulated at 60 °C for 100 s. Light detection was done using standard photo multiplier tube (PMT), bi-alkali EMI 9235QA, coupled to Hoya U-340,Schott BG-39 and Corning 7–59 optical filters.

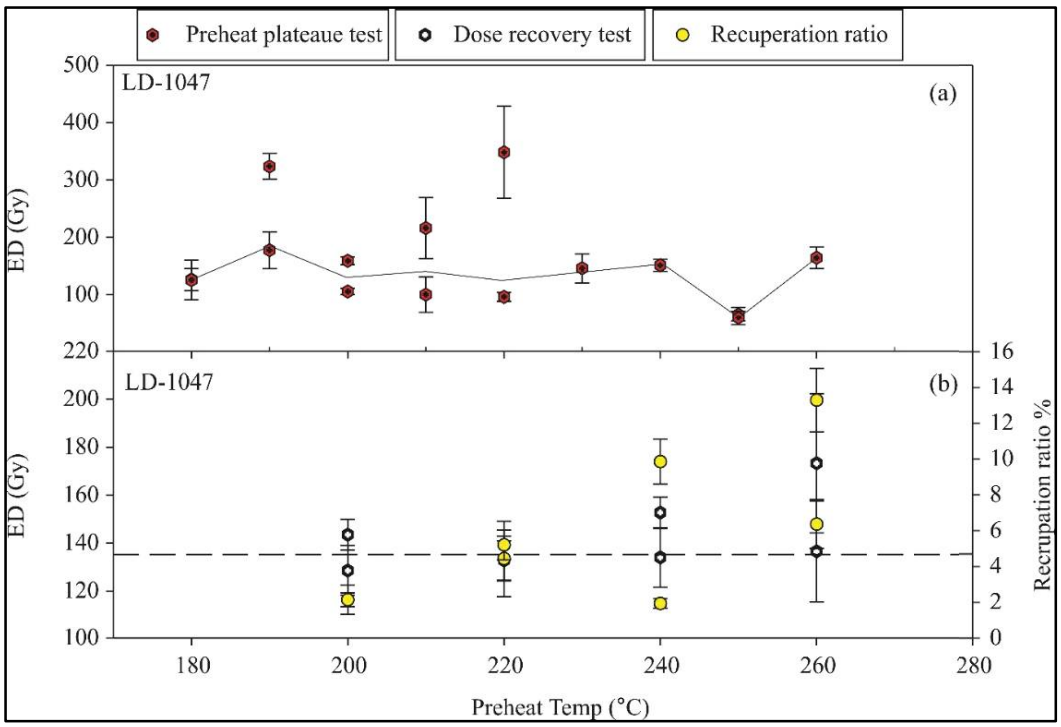

Figure 2.6 The preheat plateau and dose recovery tests were subjected to LD-1047 to know the suitable preheat temperature for applicability of SAR protocol. (a) In preheat plateaue test, the stability in the observed palaeodose at preheat temperatures between 200° and 240° C. At temperature lower than 180° C and higher than 240° C shows small gradient. This test suggest the temperature in between 200° - 240° C are suitable for SAR. (b) In dose recovery test, the given dose was extracted at different preheat temperature. At higher temperatures, the palaeodose scattering and recuperation ratio exceeded from the acceptable limit. The lower temperatures having least recuperation ratio and less scattering, therefore 220° C is used as preheat temperature.

A 5-points SAR protocol with preheat of 220 °C/10 s and cut heat of 160 °C was followed for palaeodose estimation (Murray and Wintle, 2000). The palaeodose of 30-35 discs was calculated by counting photons of initial 5 channels (1 channel = 0.16 s) of the shine-down curve. The applicability of preheat temperature and SAR protocol was satisfactory tested by preheat plateau and low recuperation (<5%), dose recovery test and recycling ratios (Fig 2.6). A threshold of recycling ratio 1±0.1 was also applied to all aliquots, if the values cross the limit then it was rejected. The weighted mean and least 20 % of palaeodoses were utilized for age calculations.

2.4.6 Problems in samples from Ladakh

Two main problems were faced while establishing OSL chronology of samples collected from Ladakh. First, the high energy fluvial environment might have led to inhomogeneous or partially bleaching that potentially overestimates ages and higher spread in palaeodose distribution. The positively skewed distribution of palaeodoses of Ladakh samples represents the partially bleaching (Olley et al., 1999; Srivastava et al., 2009; Ray and Srivastava, 2010). Therefore, correction were applied and minimum age model was applied (the least 20 %). The concept of minimum age model is based on the assumption that the quartz grains, which have lowest palaeodose are sufficiently bleached. Hence, the minimum 20 % palaeodoses were used for final age calculations on sand ramp samples (Fig 2.7) (see Srivastava et al., 2006, 2008, 2009; Ray and Srivastava, 2010).The samples from valley fill and strath terraces were subjected to statistical methods to ascertain

the degree of bleaching of the quartz. This was done by measuring the scattering of palaeodose and standard deviation from the mean palaeodose (Clarke, 1996; Colls et al., 2001). The coefficient of variation (S_n) is the ratio of standard deviation to the mean palaeodose, which significantly used for degree of bleaching: S_n, < 0.05, well-bleached; 0.05-0.1, moderately well bleached; 0.1 – 0.15, moderately partially bleached; > 0.15, partially bleached (Clarke, 1996). The values of S_n for palaeodoses scattered from 0.075 to 0.338 (scattering of Eds 7.5 % to 33.8 %), which does not mean that the scattering in the ED is due to mixing of well bleached and poorly bleached grains. Therefore, another approach is needed to discriminate the well bleached and poorly bleached grains. The correlation coefficient (R^2) palaeodose of every aliquot and their respective natural intensities detect the bleaching history (Colls et al., 2001). In well bleached samples, the natural intensity of luminescence of every aliquot may vary from other, but their palaeodoses will scatter within the error limits. Therefore, the correlation coefficient (R^2) can be used as a tool to detect the degree of bleaching. The values of $R^2 < 0.6$ refers to well bleached and > 0.6, partially bleached. The samples that show low correlation R^2 were considered well bleached where higher S_n values were considered as differential dose responses. In such case, 'central age model' was used to evaluate the ages, otherwise, in samples showing characteristics of poor bleaching 'minimum age model' was employed . Secondly, the Himalayan quartz has low

sensitivity and also at times show significant feldspar contamination (Ray and Srivastava, 2010).

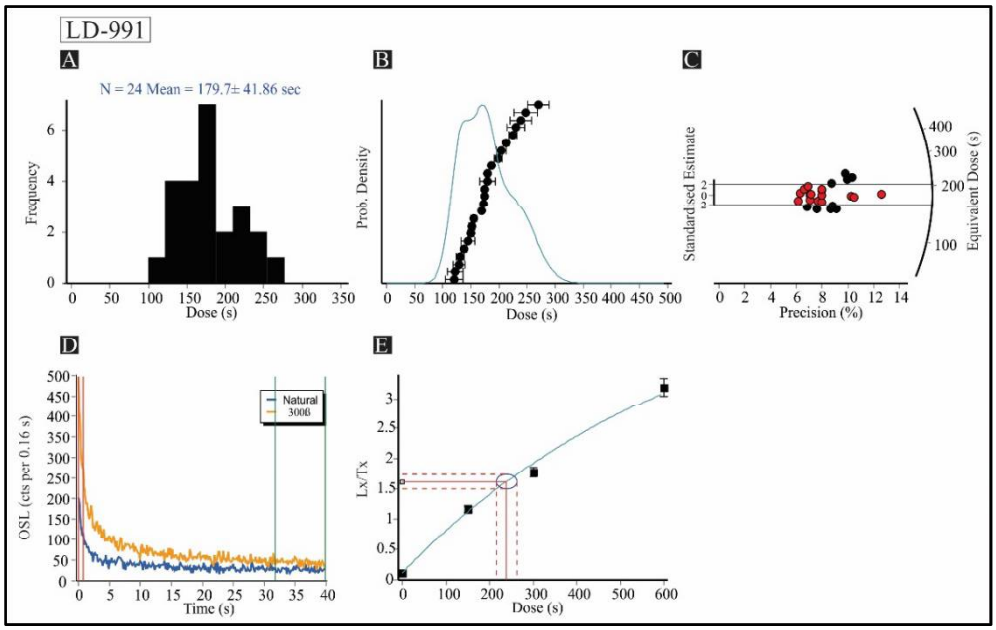

Figure 2.7 (A) and (B) Histogram and positively skewed weighted mean dose distribution showing partial bleaching of sample from Biamah section, (C) the rectangle in the radial plot representing the weighted mean palaeodoses used for age calculation, (D) the shine down curve, and (E) the growth curve for the same sample.

By reducing the aliquot size from 10 mm to 4 mm diameter that leads to increase the probability of picking up the OSL signals from maximum bleached quartz grains. However, owing to low photon counts smaller aliquots could not be used. The OSL dates from all studied sections are given in Table 2.2.

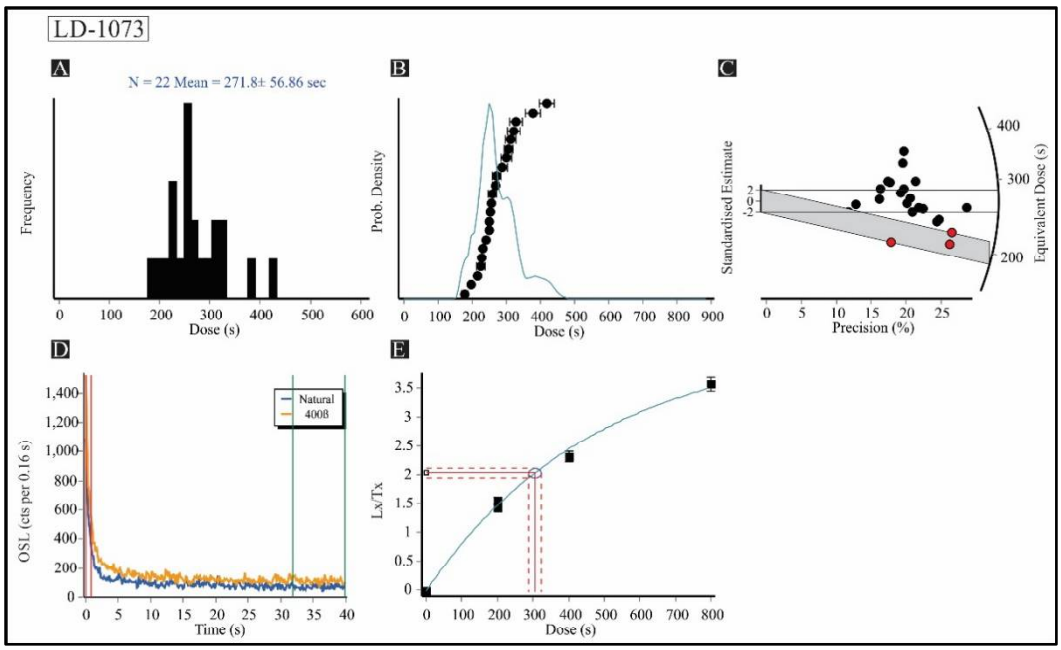

Figure 2.8 Histogram and frequency distribution curve of sample from Saboo sand ramp are represented in (A) and (B). (C) In radial plot, the hollow rectangle bar represents the mean, whereas the shaded bar represents the least 20 % palaeodoses, which was considered for age calculation, (D) the shine down curve showing no feldspar contamination in this sample, and (E) the growth curve for the same sample.

2.5 Environmental Magnetic Parameters

Environmental magnetic parameters are most commonly used to understand the erosional history and processes, climate change, pedogenesis and other paleoenvironmental studies in the Quaternary time. The commonly occurred magnetic minerals are very sensitive to climate change, transport media and

depositional setting (Sangode et al., 2007). The measurement of inherent properties of magnetic minerals through different parameters can provide an information related to mineral occurrence and surface processes which these minerals have endured. Bulk magnetic susceptibility (χlf) measures the concentration of +Remnant Magnetism (SIRM) is also measure the magnetic minerals concentration and is a function of mineral size. Anhysteretic Remnant Magnetism (ARM) indicator of fine grained stable single domain (SSD) magnetic minerals. S_{ratio} has the capability to distinguish the ferromagnetic and antiferromagnetic minerals of varied size admixture of sediment sample. The environmental magnetic parameters were measured on forty three sediment samples of Saboo sand ramp. The sampling was done at 10 cm interval in 4.5 m thick section. A fraction of well mixed sediment was packed in 10 cm^3 non- magnetic styrene vessel. χlf at low and high frequencies (0.47 and 4.7 kHz) along six directions using Bartington MS 2B laboratory sensor were measured. An ARM was developed with peak alternating field of 100 mT in the presence of DC field 0.1 mT. The Isothermal Remnant Magnetism (IRM) was measured at impulse magnetizer in both forward and backward fields 50, 100, 300, 500, 600, 800, 1000, 1200 mT and -10, -20, -30, -50, -100, -300, -400 mT respectively. The IRM_{1000} was referred as a point of Saturation Isothermal Remnant Magnetism (SIRM). The S_{ratio} was calculated by taking negative ratio of IRM_{-300} and SIRM (Basavaiah and Khadkikar, 2004; Evans and Heller 2003).

2.6 X-ray Diffraction for clay minerals

Sediment samples from the Saboo sand ramps were also analyzed for clay mineralogy using X-Ray Diffractometer (XRD). A known weight of these samples were sieved on automated sieve shaker following standard procedures given by Carver (1971). Fraction < 63 μm was subjected to Stoke's law of gravity settling to separate total clay faction (~ 2 μm). A ~ 30 mg of sample was pipetted out after from the depth of 5 cm at fixed timing and ambient temperature. The standard chemical pretreatment were followed given by Srivastava et al. (1998). The oriented clay slides were exposed to X-ray sequentially to air dried, glycolated and heated at 110 °C, 300 °C and 550 °C, on Phillips X-ray unit (PW 1729) having Ni filtered Cu radiation (Cu K α) target (Srivastava et al., 1998; Suresh et al., 2004). The clay minerals are identified by their d – spacing and diffraction patterns at sequential XRD analysis (Hillier 2003; Suresh et al., 2004).

Table 2.2 Sample locations, dosimetry, weighted mean palaeodose, dose rate and mean ages of all the samples from the Indus River

Lab No	Field Name	Latitude	Longitude	Depth (m)	U (ppm)	Th (ppm)	K %	Cosmic Dose rate (µGy/a)	Wt. mean Palaeodose (Gy)	Dose Rate (mGy/a)	Mean Age (ka)
Mahe											
LD-1433	IR-1	N 33°16'5.2"	E 78°28'7.4"	9.63	3.17	5.2	1.9	254±76	42±7	3.1±0.1	14±2
LD-1047	IND-15	N 33°17'3.8"	E 78°25'16.6"	8	2.5	10.1	2.4	274±81	154±6	3.8±0.1	41±2
Niornis											
LD-1048	IND-16	N 3°25'58.4"	E 78°11'56.1"	5	8.6	9.3	2.7	299±90	106±15	3.8±0.2	28±4
Kiari											
LD-1063	IND-17	N 3°28'11.5"	E 78°8'40.2"	12	2.3	8	2.2	241±72	88±12	3.4±0.2	26±4
Gaik											
LD-1064	IND-18	N 33°34'17"	E 78°7'31.8"	20	4.1	11	2.6	217±65	58±5	4.4±0.2	13±1
LD-1065	IND-19	N 33°34'17"	E 78°7'31.8"	7	3.5	16.1	2.9	268±80	74±7	4.9±0.2	15±1
Tirido											
LD-1066	IND-20	N 33°35'4.1"	E 78°4'57.7"	16	2.9	8.5	2.1	223±67	100±12	3.5±0.2	29±3
LD-1067	IND-21	N 33°35'4.1"	E 78°4'57.7"	0.5	2.5	5.6	2.5	372±112	102±6	3.7±0.2	26±2
Hymia-1											
LD-1068	IND-22	N 3°39'58.6"	E 77°59'44.7"	7	2.2	15	3.1	260±78	117±5	4.7±0.2	24±1

LD-1069	IND-23	N 3°39'58.6"	E 77°59'44.7"	13.5	2.9	13.4	2.3	225±68	91±7	4.0±0.2	23±2
Hymia-2											
LD-1434	IR-2	N 3°40'45.2"	E 7°59'16.88"	20.7	5.08	7.3	2.2	260±78	28±4	4.0±0.2	7±1
LD-1435	IR-3	N 3°40'45.2"	E 7°59'16.88"	24	6	21.1	2.6	221±22	71±12	5.6±0.2	13±2
Upshi											
LD-1070	IND-24	N 3°47'22.1"	E 77°51'8.3"	10	1.4	7.7	1.6	237±71	108±8	2.9±0.1	37±3
LD-1046	IND-14	N 33°49'49"	E 77°48'45.5"	15	2.3	21.1	2.7	212±63	145±7	4.8±0.2	30±2
Kharu											
LD-1045	IND-13	N 3°54'56.9"	E 77°44'4"	3	2.0	12.1	2.6	295±89	131±6	4.0±0.2	33±2
Stakna											
LD-1015	IND-8	N 3°57'30.7"	E 77°42'46.5"	7	1.5	7.9	1.9	245±75	137±4	2.9±0.2	47±1
LD-1016	IND-9	N 3°57'30.7"	E 77°42'46.5"	5	2.2	10.7	2.1	264±78	98±4	3.5±0.1	28±1
LD-1044	IND-12	N 3°57'35.5"	E 77°42'57.6"	3	2.7	16.4	2.9	292±87	121±7	4.8±0.2	25±1
Stakna 1											
LD-1017	IND-10	N 3°57'35.5"	E 77°42'57.6"	8	2.6	11.8	2.0	238±72	103±5	3.5±0.1	29±1
LD-1043	IND-11	N 3°57'35.5"	E 77°42'57.6"	3.5	1.1	8.6	1.8	264±78	84±4	2.8±0.1	30±1
Stakna 2											
LD-985	IND-25	N 34°00'11"	E 77°41'44.5"	10	1.9	8.3	1.6	226±68	89±23	2.9±0.1	31±8
LD-986	IND-26	N 34°00'11"	E 77°41'44.5"	11	4.0	8.9	1.7	221±66	157±24	3.4±0.1	46±7
Spituk											
LD-1003	IND-47	N 4°7'50.69"	E 77°03'30.9"	18	1.1	8.5	1.8	199±60	130±10	2.5±0.1	52±4

Nimu											
LD-1221	ZIC-1	N 4°9’57.57”	E 77°19’20.1”	8	1.9	6.2	0.7	200±60	94±10	1.7±0.1	55±6
Saspol											
LD-1000	IND-44	N 4º14’50.3”	E 77º6’40.6”	10	1.3	7	1.9	217±66	48±5	2.8±0.1	17±2
LD-990	IND-43	N 4º14’50.3”	E 77º6’40.6”	11.25	1.5	11.1	1.6	211±63	140±13	2.8±0.1	50±5
Nurla											
LD-989	IND-42	N 4º17’24.3”	E 77º2’3.4”	20	1.2	6.3	0.9	187±57	133±9	1.7±0.1	78±5
Khalsi											
LD-997	IND-39	N 4º19’33.6”	E 76º50’40”	30	1.0	12.2	1.5	179±54	140±13	2.7±0.1	52±5
LD-996	IND-38	N 4º19’33.6”	E 76º50’40”	1.5	0.7	6.4	1.4	301±90	90±8	2.2±0.1	41±4
LD-998	IND-40	N 4º19’33.6”	E 76º50’40”	4	1.3	7.6	2.1	260±78	55±4	3.1±0.1	18±1
Dumkhar											
LD-995	IND-37	N 34º23’58”	E 76º45’49.8”	9	1.2	12.9	1.7	217±66	170±9	3.0±0.1	57±3
Skyurbuchan Gompa											
LD-988	IND-36	N 34º26’0.6”	E 76º42’54.3”	15	1.5	7	2.0	195±60	163±21	2.9±0.1	56±7
Skyurbuchan Downstream											
LD-987	IND-33	N 34º27’0.6”	E 76º41’5.7”	19	1.2	6.7	1.1	187±57	149±12	1.8±0.1	83±7
LD-993	IND-34	N 34º27’0.6”	E 76º41’5.7”	4.5	1.3	8.3	1.5	253±75	117±17	2.5±0.1	47±7
Biamah											
LD-991	IND-31	N 4º36’34.9”	E 76º29’58.4”	6.5	2.1	12.4	1.4	226±69	21±3	2.9±0.1	7±1